Title
Junction Plasmon Driven Population Inversion of Molecular Vibrations: A Picosecond Surface-Enhanced Raman Spectroscopy Study.

Journal
Nano letters, 18(9)

ISSN
1530-6984

Authors
Crampton, Kevin T
Fast, Alexander
Potma, Eric O
et al.

Publication Date
2018-09-01

DOI
10.1021/acs.nanolett.8b02438

NANO LETTERS
Letter
Cite This: Nano Lett. 2018, 18, 5791−5796
pubs.acs.org/NanoLett

Junction Plasmon Driven Population Inversion of Molecular Vibrations: A Picosecond Surface-Enhanced Raman Spectroscopy Study

Kevin T. Crampton,*,† Alexander Fast,‡ Eric O. Potma, and V. Ara Apkarian*

Department of Chemistry, University of California Irvine, Irvine, California 92697, United States

Supporting Information

ABSTRACT: Molecular surface-enhanced Raman spectra recorded at single plasmonic nanojunctions using a 7 ps pulse train exhibit vibrational up-pumping and population inversion. The process is assigned to plasmon-driven, dark, impulsive electron-vibration (e-v) excitation. Both optical (Raman) pumping and hot-electron mediated excitation can be rejected by the characteristic spectra, which allow the simultaneous measurement of vibrational temperature of the molecules and electronic temperature of the metal. Vibrational populations are determined from anti-Stokes to Stokes intensity ratios, while the electron temperature is obtained from the anti-Stokes branch of the electronic Raman scattering continuum. Population inversion survives in high-frequency vibrations that effectively decouple from the metal.

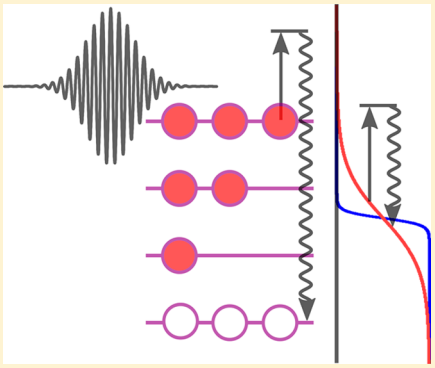

KEYWORDS: *Surface-enhanced Raman, Stokes-to-anti-Stokes ratio, population inversion, plasmon, vibrational population*

Plasmonic nanojunctions effectively confine optical fields on the angstrom scale. This is most directly demonstrated in tip-enhanced Raman spectro-microscopy (TER-sm) carried out at the precisely controllable junction of scanning tunneling microscopes (STM), where the imaging of single molecules (SM) with submolecular spatial resolution is attained.[1−3] Although it is recognized that confinement of optical fields is key to SM vibrational spectroscopy, TER-sm establishes that the operative length scale of the interactions between tip and molecule is on atomic scales. On such scales, optical fields cannot be separated from the charge-density oscillations that drive them. Disentangling the interplay between electron versus the photomediated coupling of molecules and plasmons is necessary to clarify principles of surface-enhanced spectroscopies and, more generally, of plasmon-driven molecular chemistry and physics.

The above considerations are also of interest in time-domain measurements of vibrational dynamics, which, in the SM limit, are commonly achieved through surface-enhanced coherent Raman scattering processes and fluorescence schemes.[4−6] While frequency-domain SM surface-enhanced Raman scattering (SERS)[7−17] and TER-sm[1−3,18−20] measurements abound, including measurements with ultrafast pulses,[4,21,22] their time-domain implementation has proven to be challenging. The challenge can be attributed, in part, to the impulsive scattering of surface plasmons on molecular adsorbates, which leads to the efficient up-pumping of molecular vibrations. This can be readily concluded from the anomalous anti-Stokes-to-Stokes (AS-to-S) intensity ratios seen in SERS spectra recorded with picosecond (ps) pulses and their contrast with continuous-wave (cw) spectra, which we present in this work. The interpretation is further corroborated by simultaneous surface-enhanced stimulated Raman (SESRS) and coherent anti-Stokes Raman scattering (SECARS) measurements recorded on plasmonic nanosphere dimers, which we describe below.

Anomalous AS-to-S ratios in SERS are commonly observed.[8,15,23−29] They are typically considered in the context of thermal versus optical pumping,[8,30] and in specific cases, electronic mechanisms have been proposed.[25,31] The thermal mechanism raises the question of equilibration between the temperature of the molecule and metal, recognizing that the latter may sustain distinct electronic and lattice temperatures.[32−37] The optical pumping mechanism is associated with enhanced Raman scattering, with S and AS rates that may differ due to the spectral overlap of transitions with the acting plasmonic or cavity resonances. We propose that the commonly accepted damping mechanism of plasmons by scattering on surface adsorbates serves as an efficient dark channel for the impulsive up-pumping of molecular vibrations, i.e., through electron-vibration (e-v) excitation. This mechanism can explain many of the anomalies observed in both time and frequency domain studies utilizing surface enhancement.

The measurements are carried out on the nanoscale analog of the Hertzian dipolar antenna, which consists of gold-nanosphere dimers. The commercially obtained nanodumbbells (Cabot, Inc.) are laced with 1,2-di(4-pyridyl)ethylene

Received: June 15, 2018
Revised: July 18, 2018
Published: July 31, 2018

DOI: 10.1021/acs.nanolett.8b02438
Nano Lett. 2018, 18, 5791−5796

(BPE) molecules and then encapsulated in silica (shell thickness of 40−70 nm). This system enables Raman spectroscopy in the few- to single-molecule limit by virtue of the nanoscopic focal volume at the intersphere junction. The nominal diameter of the nanospheres is 95 nm with intersphere gaps that vary from 1−0 nm. The latter is established by a sampling of dark field spectra recorded on individual nantennas, presented in Figure 1. The spectral shift of the

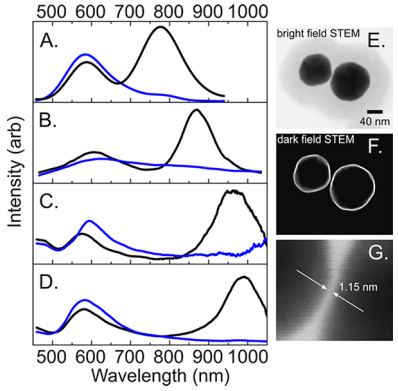

Figure 1. (A−D) Dark-field spectra recorded on individual nanodumbbells with polarization along long (black traces) and short (blue traces) axes. High-resolution electron micrographs of the dumbbell corresponding to the spectrum in panel A are shown in panels E and F. Bright- and dark-field STEM collection geometries provide the nantenna with gross morphology and junction fine structure, which is shown in panel G. The latter reveals a physical gap of 1.15 nm.

binding dipolar plasmon (BDP) resonance, from 775 to 1000 nm in the spectra of Figure 1, is a unique indicator of the gap. This is illustrated in Figure 2 by the simulated extinction spectra using generalized multiparticle Mie (GMM) theory.[38,39] The direct measurement of the junction gap through conventional electron microscopy is not reliable because the required electron flux commonly induces fusion. To cross-check the validity of the spectral determination, we

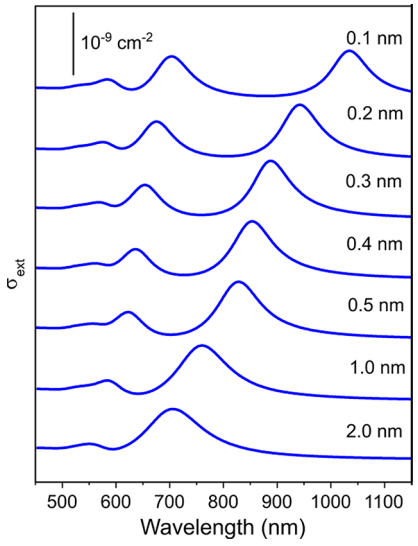

Figure 2. Calculated gap-dependent extinction spectra for an Au dimer of 95 nm diameter embedded in a homogeneous medium with a dielectric constant of 1.25.

use cryo-scanning transmission electron microscopy, with the sample held at 80 K. The micrographs of the nanodumbbell in Figure 1E−G establish a gap of 1.15 nm. Its BDP resonance appears at 775 nm (Figure 1A), in good agreement with the simulated spectrum for a 1 nm gap (see Figure 2). The implied junction gaps for particles B−D in Figure 1 are 0.4, 0.2, and 0.16 nm. Noting that the diameter of a gold atom is 0.34 nm, the junction gaps are commonly subatomic. In this limit, the classical estimates provided through GMM are approximate because they do not account for quantum effects identified in similar plasmonic constructs.[40,41]

SERS spectra recorded on different nanodumbbells, under cw and pulsed excitation with a 7 ps pulse train, are presented in Figure 3. Stokes and anti-Stokes branches are simultaneously recorded using a notch filter to block the Rayleigh line. An additional band-pass filter is used in the ps-SERS spectra, which is responsible for the roll-off at the spectral shift of ± 1900 cm^{-1}. As expected, under cw illumination, the nantenna and its molecular load appear to be in thermal equilibrium. This is established by the cw-SERS spectrum, where, in addition to the vibrational lines of the molecule, the electronic Raman scattering (ERS) spectrum of the metal can be seen (gray trace in the magnified AS branch of Figure 3Ai). The profile of the ERS is determined by the joint density of electron−hole states, which for large spectral shifts ($\hbar\omega = E_e - E_h$) reduces to the Boltzmann distribution.[42−44] The profile can be fitted to:

$$I_{ERS}(\omega) = \omega^3 e^{-\hbar\omega/k_B T_e} \quad (1)$$

to extract the electron temperature. This is highlighted in Figure 3B, where the ERS profile is shown isolated from the molecular lines and fitted to eq 1. The extracted temperature $T_e = 385 \pm 5$ K agrees with the vibrational temperature of the molecule, obtained from the AS-to-S intensity ratios of the vibrational lines:

$$\frac{I_{AS,v}}{I_{S,v}}\left(\frac{\omega_S}{\omega_{AS}}\right)^3 = e^{-\hbar\omega_v/k_B T_v} = \frac{N_{v=1}}{N_{v=0}}. \quad (2)$$

The five prominent pairs of lines seen in the spectrum of Figure 3Ai yield a mean vibrational temperature of $T_v = 394 \pm 20$ K. The consistency is highlighted by logarithmic plots of the AS-to-S intensity ratios for these lines and for the metal, computed using eq 2 and the measured value of $T_e = 385 \pm 5$ K, which are shown in Figure 3C. Note the cubic weighting of the observed intensities in eqs 1 and 2 as opposed to the quartic dependence that has appeared in recent analysis of the same (see the justification in Supporting Information).[24,27,45−47] eq 1 seems to hold over the 3000 cm^{-1} range spanned by the vibration pairs. Consistent with this, the AS-ERS continuum does not show any spectral structure due to plasmon resonance(s) appearing in this range, as would be expected if nantenna resonances enhanced ERS rates. This holds for over 30 nanodumbbells investigated through their cw-SERS spectra, both at 532 nm and at 633 nm excitation, which flank the transverse and longitudinal resonances seen in Figures 1 and 2. In contrast with the AS-ERS, which is depolarized, the Stokes branch of the continuum is polarized and tracks the polarization of the molecular lines.[42] It can be assigned to multipolar resonant Raman scattering on the junction plasmon resonances. This assignment has also been recognized in a recent study of the related system of nanoparticle-on-mirror, where direct correlation between the

DOI: 10.1021/acs.nanolett.8b02438
Nano Lett. 2018, 18, 5791−5796

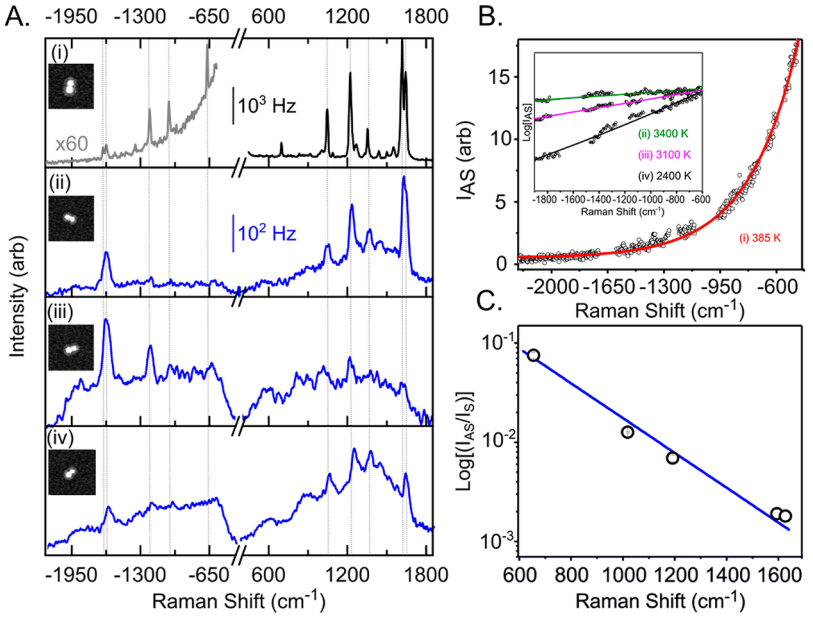

Figure 3. (A) SERS spectra recorded on single nantennas via (i) continuous wave excitation (633 nm, 30 $\mu W/\mu m^2$) and (ii–iv) pulsed excitation (785 nm, 7 ps, 76 MHz, 100 $\mu W/\mu m^2$). In all cases, the polarization of the incident field is aligned with the long axis of the dimer. Micrographs of each dimer, acquired after the SERS measurements, are shown in the insets. (B) Anti-Stokes branch of the ERS continuum for cw excitation (open circles) and pulsed excitation (inset) after removing the molecular lines. The fits to eq 1 of text (continuous lines) yield metal electronic temperatures of 385, 3400, 3100, and 2400 K for the spectra shown in panels i–iv, respectively. (C) S-to-AS ratios extracted from the five prominent vibrations of BPE (open circles) and the predicted ratios, assuming equilibration between metal and molecule and using the measured electronic temperature of 385 K (blue trace; see eq 2).

Stokes continuum and dark field spectra could be demonstrated over a large spectral tuning range.[48,49] Given the spectral variations on different dumbbells illustrated by the dark field spectra of Figure 1, it would seem that the SERS rates are not trivially correlated to the plasmonic resonances seen in extinction spectra. The same is implied by the utility of eq 2, which is otherwise only rigorously valid for normal, spontaneous, nonresonant Raman scattering.

The contrast between cw-SERS and ps-SERS spectra is striking. The intensity in the molecular AS channel has increased by 3 orders of magnitude, scaling with the peak intensity of the picosecond excitation. The electronic temperatures are significantly elevated, as is evident by the slopes of the AS-ERS continua (inset to Figure 3B). Fits of the ERS background to eq 1 yield electronic temperatures of T_e = 2400 ± 100, 3100 ± 280, and 3400 ± 160 K for the spectra in Figure 3Aii–iv, respectively. The molecular vibrational populations are athermal; moreover, in the spectrum of Figure 3Aiii, the vibrational populations can be seen to be inverted. This is clearest for the 1600 cm^{-1} mode, which, after correction for instrumental response, yields $N_{v=1}/N_{v=0}$ = 2.2. (T_v = −3000 K). While the 1250 cm^{-1} mode is not inverted, its population ratio $N_{v=1}/N_{v=0}$ = 0.52 corresponds to T_v = +3400 *K*, comparable to the electron temperature, T_e = 3100 K, of the metal. While in the thermally equilibrated cw-SERS spectrum intensities of AS lines are progressively lowered as a function of vibrational energy, the opposite trend holds in the picosecond spectra. The highest-energy states carry the intensity, while the lower lines blend in the ERS of the hot electrons; the most-prominent molecular AS line in the cw spectrum at 650 cm^{-1} is completely absent in the ps-SERS spectra. Remarkably, there is no correlation between the observed electronic and vibrational temperatures among the different dumbbells. The vibrational up-pumping effect is specific to different structures, presumably due to variations in the atomistic morphology of the nanojunction and location of the molecule in the nanocavity.

It is fairly easy to be convinced that the molecular vibrations are not optically pumped. To be able to see AS lines in the ps-SERS spectra, ν = 1 must be prepared and interrogated within the 7 ps duration of the pulse. For the Stokes radiation, either the molecular SERS or the ERS, to be effective in optical pumping, a scattering rate of ~10^{11} s^{-1} is required. As indicated by the scale bars in Figure 3A, the observed average scattering rates are ~10^3 s^{-1}, which, after accounting for the fill-factor of the picosecond pulse train, correspond to 2 × 10^6 s^{-1}, nearly 5 orders of magnitude short of the required scattering rate. Indeed, Raman pumping may compete with the thermal occupation of vibrational states upon resonant excitation of bright dyes, which is convincingly demonstrated at cryogenic temperatures.[23] The effect is negligible in the present nonresonant SERS governed by electromagnetic enhancement factors. The Raman cross-section of the brightest vibrational mode in BPE is σ_s = 5 × 10^{-28} cm^2 and the operative overall enhancement factor of 10^8 is sufficient to observe single molecules but not enough to drive the system away from thermal equilibrium. Optical pumping schemes have been advanced in terms of nanocavity optomechanics.[15,31] The governing kinetic equations are not different from those used to treat optical pumping through SERS under plasmonic resonances.[50] Given the relatively low cavity quality factors, these mechanisms are difficult to reconcile with population inversion of a selected mode, the observed electron temperatures, or the essential requirement of an enhancement factor of 10^{13} for SERS rates to compete with vibrational relaxation rates. The observed vibrational population through the AS spectrum must be prepared through a dark channel.

DOI: 10.1021/acs.nanolett.8b02438
Nano Lett. 2018, 18, 5791–5796

The vibrational up-pumping observed in the ps-SERS spectra is efficient. Because the pulse duration is comparable to the vibrational lifetime of the mode, only a fraction $\sim (1 - e^{-1})$ of the nascent population in $\nu = 1$ is captured in the spectra. The correction implies that the nascent population ratio in the inverted 1600 cm^{-1} mode is $N^0_{\nu=1}/N^0_{\nu=0} \geq 3.5$. In the single-molecule limit, this implies that $\sim^3/_4$ of the pulses in the 76 MHz train prepare the excited state. Summed over all vibrations, it can be concluded that the vibrational up-pumping is driven with unit probability per pulse. Damping of the plasmon by its impulsive scattering on the molecule is the likely mechanism that contains the necessary bandwidth to prepare the observed vibrations. This occurs in parallel with the electron−electron (e−e) scattering channel that creates the hot electron−hole (e−h) pairs seen in the ERS continuum. To develop a line spectrum, the vibration must be decoupled from the electron gas. As such, the hot electrons do not appear to prepare or damp the molecular vibration. While the electrons are continuously excited under the pulse, the 1600 cm^{-1} mode must be prepared and survive for the duration of the pulse to yield the observed line width. Thermal equilibration between metal and molecule should be mediated by the lattice phonons, which are heated through electron−phonon relaxation on ∼2 ps time scales.[32−36] Consistent with this expectation, only vibrations with energy significantly above the phonon bath temperature live long enough to form line spectra, which explains the preferential inversion of higher-frequency modes and the absence of low-lying vibrations in the AS spectra. This is consistent with a recent report of decoupled electronic and vibrational temperatures in SERS.[47] A dark impulsive electronic to vibrational excitation (e-v) channel, followed by vibration to phonon (v−ph) energy exchange, is implied by the ps-SERS spectra.

Plasmon-mediated impulsive vibrational excitation explains observations made in the ultrafast time domain studies of molecules at nanojunctions.[4] We highlight this through simultaneous SRS and CARS measurements carried out with the picosecond pulse train. The experimental arrangement, which has been described previously,[43] is included in the Experimental section. The particular measurements are carried on an ensemble of dry-mounted, well-dispersed nanoantennas, which contain a distribution of dimers and larger aggregates. The SRS signal is tracked as a loss in the pump pulse, while the CARS signal is recorded in the backscattered channel. We show in Figure 4 the simultaneously recorded SRS and CARS data. The SRS channel carries a large signal, which, however, is entirely featureless. The CARS channel shows the 1600 cm^{-1} doublet previously recorded on individual dumbbells.[43] SRS requires phase-coherent preparation of the vibrational packet, which apparently is not achieved. CARS interrogates the SRS prepared packet through the same AS scattering process as in the ps-SERS spectra. The requirement of coherence between preparation and interrogation to develop the CARS signal in ensembles is entirely relaxed in the single molecule limit. As long as $\nu = 1$ is prepared by the pump and dump pulses, the AS scattering signal can be seen because single molecules are impervious to pure dephasing. In the strong coupling regime, the preparation imparts a stochastic phase, which does not prevent detection through AS-Raman scattering.[4]

The identified plasmon-driven, dark, impulsive e-v excitation channel explains observations common to a range of enhanced spectroscopies and plays an important role in single-molecule time-domain measurements because it mimics broad-band impulsive Raman pumping. Although optically driven, the e-v energy-transfer mechanism is distinct from all-optical (Raman) pumping by the absence of a carrier phase. This distinction is nicely highlighted in the simultaneously recorded SRS and CARS traces. Despite the strength of the SRS signal, it carries no spectral information because the required phase coherence between pump and dump pulses cannot be sustained for the 7 ps duration of the two pulses. However, the mechanism allows SRS with temporally mismatched femtosecond−picosecond pulse pairs, as was already demonstrated on the same nantennas.[51−54] Because CARS in the single-molecule limit does not require phase coherence between preparation and interrogation of vibrations, it yields spectra with normal line shapes.

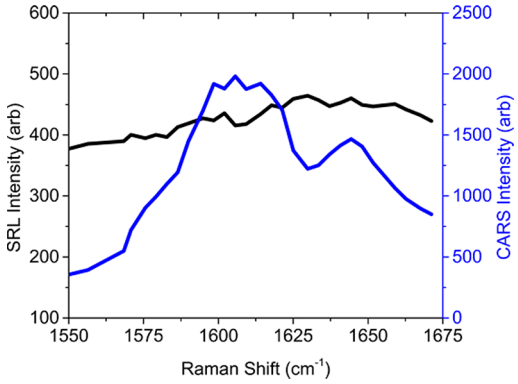

Figure 4. Simultaneously recorded SRS and CARS on an ensemble of nantennas. The CARS channel tracks the 1604 and 1640 cm^{-1} modes of BPE. The featureless SRL channel reflects the lack of phase coherence between the interrogating pulse and the electron-mediated vibrational preparation.

Rather than the plasmonic field, the coherent charge oscillations that carry the field do the work in the e-v pumping mechanism. Indeed, at atomistic junction gaps, the local fields are displacements, $D = E + 4\pi P$, where the polarization includes the extended plasmon and local contacts between molecule and metal. Similar conclusions can be reached in a variety of closely related experiments in existing literature accounts. For example, the inverted AS-to-S ratios and preferential up-pumping of high-frequency modes was recently reported in a nonresonant molecule under cw excitation[45] and associated with individual atom−molecule contacts to rationalize the inversion under steady-state excitation. The overall absence of coloration in the SERS spectra obviates mechanisms due to cavity resonances and optomechanical pumping.

Clearly, the e-v mechanism can be dramatically amplified through metal-molecule charge transfer or interfacial resonances, which are directly addressed in time-resolved photoelectron emission spectroscopy[55] or indirectly through the observation of transient ion formation.[56] The mechanism can also be regarded as a natural outcome of plasmon electron-density permeating through surface attached ligands.[57] Overall, these measurements clarify the mechanism of vibrational population preparation and metal−molecule coupling in plasmon-enhanced spectroscopies.

Experimental Section. *CARS and SRS Spectro-microscopy.* These experiments were performed using a conventional inverted optical microscope equipped with galvo scanning mirrors. For single-particle SRS and CARS measurements, the microscope was coupled to a coincident pair of 76 MHz pulse

DOI: 10.1021/acs.nanolett.8b02438
Nano Lett. 2018, 18, 5791−5796

trains of 7 ps duration, emanating from the tunable output of an Nd:vanadate pumped optical parametric amplifier (Pico-Train, High-Q; Emerald OPO, A.P.E.), which served as a pump/probe pulse. The remaining fundamental output at 1064 nm was modulated at 10 MHz and served as the Stokes pulse. The collinear pump and probe pulse train was focused at the object plane via a high numerical aperture objective lens (40× oil, 1.32 NA). Images were obtained by raster scanning the excitation pulse train in the *xy* plane at a rate of 10 μs per pixel over an area of 100 μm × 100 μm while recording the transmitted or reflected probe in the forward or backscattered directions, respectively. The forward scattered probe was collected with a 1.45 NA oil condenser and focused onto a reverse biased silicon photodiode (Thorlabs Inc., FDS100). The signal was amplified by 60 dB using a voltage preamplifier (Femto Inc., HVA-10M-60-B) and demodulated at 10 MHz with a lock-in amplifier (Zurich Instruments Inc., HF2LI). CARS spectra were acquired in the epi-direction, as previously described.[43]

Pulsed and cw-SERS. SERS spectra were acquired in the backscattered direction by separating source and Raman photons with dichroic beam splitters that were matched to the excitation wavelengths of 785 nm (pulsed) and 633 nm (cw). Paired notch filters were also included in the collection path for further filtering of the source. A cooled camera spectrograph (Andor iDus 401, Shamrock SR303i) equipped with a 300 lines per millimeter grating was utilized for acquiring spectra. Typical integration times were 1 s for cw and 30 s for ultrafast excitation. The galvo mirrors were used to reposition the excitation laser for targeting individual dimers. By the recording of the SERS in the backscattered geometry, signal photons were relayed to the spectrograph via the excitation galvos. This ensured that the system remained telecentric and permitted Raman acquisition from individual, diffraction-limited objects in the focal volume.

Generalized Multi-particle Mie. The gap-dependent spectral calculations we performed using a community-sourced implementation of the GMM code.[39] Expansion coefficients up to 40th order were utilized to simulate the far-field extinction spectra for various intersphere gaps ranging from 2 to 0.1 nm. We utilized the idealized version of our experimental SERS substrate consisting of a pair of 95 nm gold spheres, modeled using the recently revised dielectric[58] and embedded in a homogeneous medium with an index of 1.25.

■ ASSOCIATED CONTENT

Supporting Information

The Supporting Information is available free of charge on the ACS Publications website at DOI: 10.1021/acs.nanolett.8b02438.

Additional details on vibrational populations and enhancement. (PDF)

■ AUTHOR INFORMATION

Corresponding Authors

*E-mail: kcrampto@uci.edu.
*E-mail: aapkaria@uci.edu.

ORCID

Kevin T. Crampton: 0000-0002-1258-7895
Eric O. Potma: 0000-0003-3916-6131
V. Ara Apkarian: 0000-0002-7648-5230

Present Addresses

†Physical Sciences Division, Pacific Northwest National Laboratory, P.O. Box 999, Richland, WA 99352, United States
‡Wellman Center for Photomedicine, Harvard Medical School, Massachusetts General Hospital, 149 13th Street, Charlestown, Massachusetts 02129, United States

Notes

The authors declare no competing financial interest.

■ ACKNOWLEDGMENTS

The authors gratefully acknowledge the skillful assistance of Toshihiro Aoki at the UC Irvine Materials Research Institute for his help with the STEM measurements. We also thank Giovanni Pellegrini for his assistance setting up the GMM calculations. This work was supported by the National Science Foundation through the Center for Chemistry at the Space-Time Limit (award no. CHE-1414466).

■ REFERENCES

(1) Tallarida, N.; Lee, J.; Apkarian, V. A. *ACS Nano* **2017**, *11*, 11393−11401.
(2) Lee, J.; Tallarida, N.; Chen, X.; Liu, P.; Jensen, L.; Apkarian, V. A. *ACS Nano* **2017**, *11*, 11466−11474.
(3) Zhang, R.; Zhang, Y.; Dong, Z. C.; Jiang, S.; Zhang, C.; Chen, L. G.; Zhang, L.; Liao, Y.; Aizpurua, J.; Luo, Y.; Yang, J. L.; Hou, J. G. *Nature* **2013**, *498*, 82−6.
(4) Yampolsky, S.; Fishman, D. A.; Dey, S.; Hulkko, E.; Banik, M.; Potma, E. O.; Apkarian, V. A. *Nat. Photonics* **2014**, *8*, 650−656.
(5) Brinks, D.; Hildner, R.; van Dijk, E. M. H. P.; Stefani, F. D.; Nieder, J. B.; Hernando, J.; van Hulst, N. F. *Chem. Soc. Rev.* **2014**, *43*, 2476−2491.
(6) Piatkowski, L.; Accanto, N.; van Hulst, N. F. *ACS Photonics* **2016**, *3*, 1401−1414.
(7) Nie, S.; Emory, S. R. *Science* **1997**, *275*, 1102−1106.
(8) Kneipp, K.; Wang, Y.; Kneipp, H.; Itzkan, I.; Dasari, R. R.; Feld, M. S. *Phys. Rev. Lett.* **1996**, *76*, 2444−2447.
(9) Jeanmaire, D. L.; Van Duyne, R. P. *J. Electroanal. Chem. Interfacial Electrochem.* **1977**, *84*, 1−20.
(10) Fleischmann, M.; Hendra, P. J.; McQuillan, A. J. *Chem. Phys. Lett.* **1974**, *26*, 163−166.
(11) Novotny, L.; van Hulst, N. *Nat. Photonics* **2011**, *5*, 83−90.
(12) Arroyo, J. O.; Kukura, P. *Nat. Photonics* **2016**, *10*, 11−17.
(13) Dieringer, J. A.; Lettan, R. B.; Scheidt, K. A.; Van Duyne, R. P. *J. Am. Chem. Soc.* **2007**, *129*, 16249−16256.
(14) Michaels, A. M.; Nirmal, M.; Brus, L. E. *J. Am. Chem. Soc.* **1999**, *121*, 9932−9939.
(15) Benz, F.; Schmidt, M. K.; Dreismann, A.; Chikkaraddy, R.; Zhang, Y.; Demetriadou, A.; Carnegie, C.; Ohadi, H.; de Nijs, B.; Esteban, R.; Aizpurua, J.; Baumberg, J. J. *Science* **2016**, *354*, 726.
(16) Albrecht, M. G.; Creighton, J. A. *J. Am. Chem. Soc.* **1977**, *99*, 5215−5217.
(17) Blackie, E. J.; Le Ru, E. C.; Etchegoin, P. G. *J. Am. Chem. Soc.* **2009**, *131*, 14466−14472.
(18) Sonntag, M. D.; Klingsporn, J. M.; Garibay, L. K.; Roberts, J. M.; Dieringer, J. A.; Seideman, T.; Scheidt, K. A.; Jensen, L.; Schatz, G. C.; Van Duyne, R. P. *J. Phys. Chem. C* **2012**, *116*, 478−483.
(19) Steidtner, J.; Pettinger, B. *Phys. Rev. Lett.* **2008**, *100*, 236101.
(20) Zhang, W.; Yeo, B. S.; Schmid, T.; Zenobi, R. *J. Phys. Chem. C* **2007**, *111*, 1733−1738.
(21) Milojevich, C. B.; Mandrell, B. K.; Turley, H. K.; Iberi, V.; Best, M. D.; Camden, J. P. *J. Phys. Chem. Lett.* **2013**, *4*, 3420−3423.
(22) Zhang, Y.; Zhen, Y.-R.; Neumann, O.; Day, J. K.; Nordlander, P.; Halas, N. J. *Nat. Commun.* **2014**, *5*, 4424.
(23) Maher, R. C.; Etchegoin, P. G.; Le Ru, E. C.; Cohen, L. F. *J. Phys. Chem. B* **2006**, *110*, 11757−11760.

DOI: 10.1021/acs.nanolett.8b02438
Nano Lett. 2018, 18, 5791−5796

(24) Maher, R. C.; Hou, J.; Cohen, L. F.; Le Ru, E. C.; Hadfield, J. M.; Harvey, J. E.; Etchegoin, P. G.; Liu, F. M.; Green, M.; Brown, R. J.; Milton, M. J. *J. Chem. Phys.* **2005**, *123*, 084702.
(25) Kozich, V.; Werncke, W. *J. Phys. Chem. C* **2010**, *114*, 10484−10488.
(26) Brolo, A. G.; Sanderson, A. C.; Smith, A. P. *Phys. Rev. B: Condens. Matter Mater. Phys.* **2004**, *69*, 045424.
(27) Maher, R. C.; Cohen, L. F.; Gallop, J. C.; Le Ru, E. C.; Etchegoin, P. G. *J. Phys. Chem. B* **2006**, *110*, 6797−6803.
(28) Pozzi, E. A.; Zrimsek, A. B.; Lethiec, C. M.; Schatz, G. C.; Hersam, M. C.; Van Duyne, R. P. *J. Phys. Chem. C* **2015**, *119*, 21116−21124.
(29) Haslett, T. L.; Tay, L.; Moskovits, M. *J. Chem. Phys.* **2000**, *113*, 1641−1646.
(30) Maher, R. C.; Galloway, C. M.; Le Ru, E. C.; Cohen, L. F.; Etchegoin, P. G. *Chem. Soc. Rev.* **2008**, *37*, 965−979.
(31) Schmidt, M. K.; Esteban, R.; Benz, F.; Baumberg, J. J.; Aizpurua, J. *Faraday Discuss.* **2017**, *205*, 31−65.
(32) Sun, C. K.; Vallée, F.; Acioli, L.; Ippen, E. P.; Fujimoto, J. G. *Phys. Rev. B: Condens. Matter Mater. Phys.* **1993**, *48*, 12365−12368.
(33) Elsayed-Ali, H. E.; Juhasz, T.; Smith, G. O.; Bron, W. E. *Phys. Rev. B: Condens. Matter Mater. Phys.* **1991**, *43*, 4488−4491.
(34) Groeneveld, R. H. M.; Sprik, R.; Lagendijk, A. *Phys. Rev. B: Condens. Matter Mater. Phys.* **1995**, *51*, 11433−11445.
(35) Schoenlein, R. W.; Lin, W. Z.; Fujimoto, J. G.; Eesley, G. L. *Phys. Rev. Lett.* **1987**, *58*, 1680−1683.
(36) Fann, W. S.; Storz, R.; Tom, H. W. K.; Bokor, J. *Phys. Rev. B: Condens. Matter Mater. Phys.* **1992**, *46*, 13592−13595.
(37) Voisin, C.; Del Fatti, N.; Christofilos, D.; Vallée, F. *J. Phys. Chem. B* **2001**, *105*, 2264−2280.
(38) Xu, Y.-l. *Appl. Opt.* **1997**, *36*, 9496−9508.
(39) Pellegrini, G.; Mattei, G.; Bello, V.; Mazzoldi, P. *Mater. Sci. Eng., C* **2007**, *27*, 1347−1350.
(40) Zhu, W.; Esteban, R.; Borisov, A. G.; Baumberg, J. J.; Nordlander, P.; Lezec, H. J.; Aizpurua, J.; Crozier, K. B. *Nat. Commun.* **2016**, *7*, 11495.
(41) Mertens, J.; Eiden, A. L.; Sigle, D. O.; Huang, F.; Lombardo, A.; Sun, Z.; Sundaram, R. S.; Colli, A.; Tserkezis, C.; Aizpurua, J.; Milana, S.; Ferrari, A. C.; Baumberg, J. J. *Nano Lett.* **2013**, *13*, 5033−5038.
(42) Dey, S.; Banik, M.; Hulkko, E.; Rodriguez, K.; Apkarian, V. A.; Galperin, M.; Nitzan, A. *Phys. Rev. B: Condens. Matter Mater. Phys.* **2016**, *93*, 035411.
(43) Crampton, K. T.; Zeytunyan, A.; Fast, A. S.; Ladani, F. T.; Alfonso-Garcia, A.; Banik, M.; Yampolsky, S.; Fishman, D. A.; Potma, E. O.; Apkarian, V. A. *J. Phys. Chem. C* **2016**, *120*, 20943−20953.
(44) Hugall, J. T.; Baumberg, J. J. *Nano Lett.* **2015**, *15*, 2600−2604.
(45) Shin, H.-H.; Yeon, G. J.; Choi, H.-K.; Park, S.-M.; Lee, K. S.; Kim, Z. H. *Nano Lett.* **2018**, *18*, 262−271.
(46) Fujimori, H.; Kakihana, M.; Ioku, K.; Goto, S.; Yoshimura, M. *Appl. Phys. Lett.* **2001**, *79*, 937−939.
(47) Keller, E. L.; Frontiera, R. R. *ACS Nano* **2018**, *12*, 5848−5855.
(48) Mahajan, S.; Cole, R. M.; Speed, J. D.; Pelfrey, S. H.; Russell, A. E.; Bartlett, P. N.; Barnett, S. M.; Baumberg, J. J. *J. Phys. Chem. C* **2010**, *114*, 7242−7250.
(49) Lombardi, A.; Schmidt, M. K.; Weller, L.; Deacon, W. M.; Benz, F.; de Nijs, B.; Aizpurua, J.; Baumberg, J. J. *Phys. Rev. X* **2018**, *8*, 011016.
(50) Le Ru, E. C.; Etchegoin, P. G. *Faraday Discuss.* **2006**, *132*, 63−75.
(51) Brandt, N. C.; Keller, E. L.; Frontiera, R. R. *J. Phys. Chem. Lett.* **2016**, *7*, 3179−85.
(52) Brooks, J. L.; Frontiera, R. R. *J. Phys. Chem. C* **2016**, *120*, 20869−20876.
(53) Frontiera, R. R.; Gruenke, N. L.; Van Duyne, R. P. *Nano Lett.* **2012**, *12*, 5989−5994.
(54) Frontiera, R. R.; Henry, A.-I.; Gruenke, N. L.; Van Duyne, R. P. *J. Phys. Chem. Lett.* **2011**, *2*, 1199−1203.
(55) Tan, S.; Dai, Y.; Zhang, S.; Liu, L.; Zhao, J.; Petek, H. *Phys. Rev. Lett.* **2018**, *120*, 126801.
(56) Sprague-Klein, E. A.; McAnally, M. O.; Zhdanov, D. V.; Zrimsek, A. B.; Apkarian, V. A.; Seideman, T.; Schatz, G. C.; Van Duyne, R. P. *J. Am. Chem. Soc.* **2017**, *139*, 15212−15221.
(57) Chen, X.; Moore, J. E.; Zekarias, M.; Jensen, L. *Nat. Commun.* **2015**, *6*, 8921.
(58) Olmon, R. L.; Slovick, B.; Johnson, T. W.; Shelton, D.; Oh, S.-H.; Boreman, G. D.; Raschke, M. B. *Phys. Rev. B: Condens. Matter Mater. Phys.* **2012**, *86*, 235147.

DOI: 10.1021/acs.nanolett.8b02438
Nano Lett. 2018, 18, 5791−5796